

Self-adapted Floquet Dynamics of Ultracold Bosons in a Cavity

Xi-Wang Luo and Chuanwei Zhang*

Department of Physics, The University of Texas at Dallas, Richardson, Texas 75080-3021, USA

Floquet dynamics of a quantum system subject to periodic modulations of system parameters provide a powerful tool for engineering new quantum matter with exotic properties. While system dynamics are significantly altered, the periodic modulation itself is usually induced externally and independent of Floquet dynamics. Here we propose a new type of Floquet physics for a Bose-Einstein condensate (BEC) subject to a shaken lattice generated inside a cavity, where the shaken lattice and atomic Floquet bands are mutually dependent, resulting in self-adapted Floquet dynamics. In particular, the shaken lattice induces Floquet quasi-energy bands for the BEC, whose back action leads to a self-adapted dynamical normal-superradiant phase transition for the shaken lattice. Such self-adapted Floquet dynamics show two surprising and unique features: *i*) the normal-superradiant phase transition possesses a hysteresis even without atom interactions; *ii*) the dynamical atom-cavity steady state could exist at free energy maxima. The atom interactions strongly affect the phase transition of the BEC from zero to finite momenta. Our results provide a powerful platform for exploring self-adapted Floquet physics, which may open an avenue for engineering novel quantum materials.

Introduction.—Floquet physics has been extensively studied in solid state, ultracold atomic, and photonic systems in recent years with significant theoretical and experimental progress [1–14]. In particular, ultracold atoms in periodically driven optical lattices provide a highly controllable and disorder-free platform for studying Floquet physics, yielding many interesting and important phenomena such as coherent ac-induced tunneling and band coupling [15–25], the realization of gauge fields and topological bands [26–37], and the dynamical control of expansion and quantum phase transition of bosonic systems [38–41], etc. These previous studies on Floquet physics assumed that system parameter modulations (e.g., the shaking or moving optical lattices) are determined solely by external driving and do not depend on system dynamics, *i.e.*, no back action of system Floquet states on parameter modulations. Therefore a natural and important question is whether novel Floquet physics can emerge when system Floquet dynamics and parameter modulations are mutually dependent.

In this Letter, we address this important question by studying Floquet dynamics of ultracold boson atoms subject to a shaken optical lattice generated inside an optical cavity. In the past several decades, the interaction between atoms and static cavity fields with atom back actions (no Floquet physics) have been well studied in both theory [42] and experiment [43–53], showcasing rich cavity quantum electrodynamics (QED) physics ranging from few-body problems such as Jaynes-Cummings model [54] to many-body physics such as the Dicke superradiance [55, 56]. However, in these studies, the cavity mode is static without periodic modulations such as shaking or moving.

Here we propose to realize a cavity-mode-induced freely evolving shaken lattice, utilizing transverse pumping and a periodic modulation of the cavity field phase, and study its mutual interaction with a non- or weakly in-

teracting Bose-Einstein condensate (BEC) inside the cavity. While such shaken lattice generates Floquet bands for the BEC, the back action of atom Floquet bands modulates the shaken lattice, leading to a dynamical superradiant phase, where atom Floquet bands and shaken lattice are self-adapted. Such Floquet normal-superradiant phase transition can be dramatically different from non-Floquet one because of the coupling between different Floquet sidebands. In particular, the interplay between intra- and inter-sideband couplings may induce a hysteresis for the Floquet normal-superradiant phase transition of non-interacting atoms, yielding a completely new mechanism different from the well-known interaction-driven hysteresis [57–62]. Surprisingly, the steady state of the atom-cavity system can stabilize at the free energy maximum for dominant inter-sideband coupling because of the non-equilibrium nature of Floquet states. With increasing superradiant field, the Floquet band dispersion gradually evolves from a single minimum to doubly degenerate minima, leading to a second-order phase transition of the BEC. Such transition can be significantly affected by the interaction between atoms through the back action, which changes the critical superradiant field, the Floquet band dispersion and the condensate momenta across the transition.

System.—As shown in Fig. 1(a), two schemes (A and B) can be used to generate shaking cavity mode as $\hat{\mathbf{z}}E(x, \varphi) \propto \hat{\mathbf{z}} \cos[k_0x + \varphi(t)]$, with $\hat{\mathbf{z}}$ the polarization direction and k_0 the wavenumber. Scheme A employs two electro-optic modulators (EOMs) [63], while scheme B uses two mirrors synchronously driven by piezoelectric transducers (PZTs) [64] to periodically and slowly [comparing with cavity free spectral range (FSR)] modify the optical phase delay by $\varphi(t) = \varphi_0 + f \cos(\omega_0 t)$. The total optical path length does not change, therefore the cavity resonance frequency is not affected. We consider a quasi-one-dimensional (the dynamics in other directions

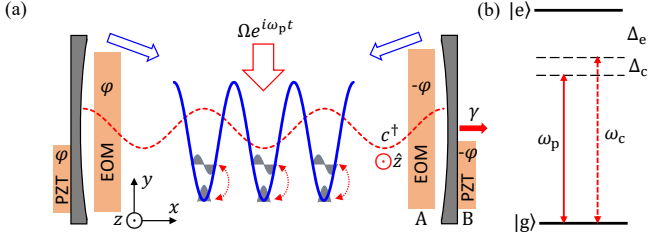


FIG. 1: (a) Schematic of the experimental setup. The cavity is pumped by an external transverse laser (red block arrow), with cavity mode (red line) shaken by the two EOMs or PZT-driving mirrors. A BEC is prepared inside the cavity with a background lattice (blue line) generated by additional lasers (blue block arrows). The shaken cavity mode may induce inter-band couplings (dotted arrows) when the band gap matches the shaking frequency. (b) Energy levels of the atom and detunings of the cavity mode and pumping laser.

are reduced by a deep harmonic trap) BEC prepared in such a cavity, which is pumped by an external transverse laser. The pumping frequency ω_p is close to the cavity resonance frequency ω_c , both of which are detuned far below the atomic transition frequency ω_a [see Fig. 1(b)].

After adiabatically eliminating the excited atomic level, we obtain the Hamiltonian of the atom-cavity system in a rotating frame with $\hbar = 1$

$$\mathcal{H} = (\Delta_c - u)c^\dagger c + \int dx \Psi^\dagger(x) H_a(t) \Psi(x), \quad (1)$$

where c is the annihilation operator of the cavity photon, and $\Psi(x)$ is the matter wave field of atoms in the ground state. $\Delta_c = \omega_c - \omega_p$ is the cavity mode detuning, and $u = \frac{g_0^2}{\Delta_e} \int dx \Psi^\dagger \Psi \cos^2(k_0 x + \varphi)$ is the detuning induced by the atoms, which is typically small and negligible. The single atom Hamiltonian is $H_a(t) = -\frac{\partial_x^2}{2m} + V_{\text{ext}}(x) + \hat{V}_c(x, t)$, with $V_{\text{ext}}(x) = v_e \cos^2(k_0 x)$ an static external background lattice potential, which can be realized by additional lasers [65]. It gives rise to a static tight-binding atomic band structure $\varepsilon_\lambda(q_x) = E_\lambda + t_\lambda \cos(q_x)$ with band index λ and Bloch momentum $q_x \in [-k_0, k_0]$ [Fig. 2(a)]. $\hat{V}_c(x, t) = -\eta \frac{c^\dagger + c}{\sqrt{N_a}} \cos[k_0 x + \varphi(t)]$ is the shaking potential induced by the cavity-assisted ac-Stark shift, with $\eta = \Omega g_0 \sqrt{N_a} / \Delta_e$ the coupling strength, $\Delta_e = \omega_a - \omega_p$ the single-photon detuning, Ω and g_0 the Rabi frequencies of the transverse pumping laser and the single cavity photon, respectively ($\Omega, g_0 \ll \Delta_e$), and total atom number N_a .

Utilizing the expansion $e^{if \cos \omega_0 t} = \sum_n i^n J_n(f) e^{in\omega_0 t}$ for $\cos[k_0 x + \varphi_0 + f \cos(\omega_0 t)]$, we see $\hat{V}_c(x, t)$ can change the band structure by inducing a sequence of sidebands (*i.e.* phonon-dressed bands) and couplings between them (see Fig. 2). We choose v_e, ω_0, φ_0 and f such that the static s -band is near resonance with two-phonon-dressed ($\omega \equiv 2\omega_0$) p -band [Fig. 2(a)], therefore only

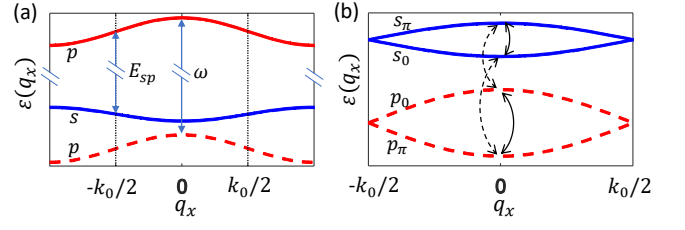


FIG. 2: (a) Illustration of atomic static bands (solid lines) and phonon-dressed sidebands (dashed lines). (b) Couplings induced by \hat{V}_c in Eq. (2). The area of the Brillouin zone reduces in half by \hat{V}_c . The time-independent (time-dependent) term induces intra-sideband (inter-sideband) couplings indicated by solid arrows (dashed arrows).

these two bands need be considered for the calculation of new Floquet band structure $\tilde{\varepsilon}_\lambda(q_x)$. The first order expansion $\propto e^{\pm i\omega_0 t}$ is far-off resonance and can be neglected. The zero-th order expansion corresponds to intra-sideband coupling, thus only terms containing $\cos(k_0 x)$ are nonzero due to the symmetry of the Wannier functions. Similarly, only terms with $\sin(k_0 x)$ are nonzero for the second-order expansion $\propto e^{\pm i2\omega_0 t}$ that couples s and p bands. In total, the cavity-assisted potential can be written as [65]

$$\hat{V}_c = -\eta_0 \frac{c^\dagger + c}{\sqrt{N_a}} [\cos(k_0 x) + 4\eta_t \cos(\omega t) \sin(k_0 x)], \quad (2)$$

where $\eta_0 = \eta J_0(f) \cos(\varphi_0)$, $\eta_t = \frac{J_2(f)}{2J_0(f)} \tan(\varphi_0)$ (tunable by f and φ_0) is the ratio between inter- and intra-sideband coupling strengths. Note that the spatial period of $\hat{V}_c(x, t)$ is twice of $V_{\text{ext}}(x)$, therefore the Brillouin zone (BZ) reduces by half to $q_x \in [-k_0/2, k_0/2]$ through the band folding. Each band λ is split into two bands λ_0, λ_π [$\lambda = s, p$ as shown in Fig. 2(b)] and the lattice potential \hat{V}_c can only couple 0 and π bands due to the momentum transfer. φ_0 characterizes the relative phase between background lattice and the shaking center of cavity field: for $\varphi_0 = 0$ ($\frac{\pi}{2}$), the shaking potential is symmetric (asymmetric) at each site of the background lattice, therefore can only induce intra-sideband (inter-sideband) couplings. Both couplings coexist for $\varphi_0 \neq j\pi/2$ (j is an integer) [65].

Method.—Under mean-field approximation, the cavity field satisfies the Langevin equation $i\langle \dot{c}(t) \rangle = \langle [c, \mathcal{H}] \rangle - i\gamma/2 \langle c(t) \rangle$ due to the weak leakage of the high-Q cavity, yielding

$$i\dot{\alpha} = (\Delta_c - u - i\gamma/2) \alpha - \eta_0 \Theta(t), \quad (3)$$

with $\alpha(t) = \langle c(t) \rangle / \sqrt{N_a}$ and γ the cavity loss rate. Here $\Theta(t) = N_a^{-1} \int dx \langle \Psi^\dagger \Psi \rangle [\cos(k_0 x) + 4\eta_t \sin(k_0 x) \cos(\omega t)]$ is the atomic density order. The frequency ω is chosen to be much larger than $\eta_0 \Theta, \Delta_c - u, \gamma/2$ (see section *experimental consideration*), so that high-order oscillation

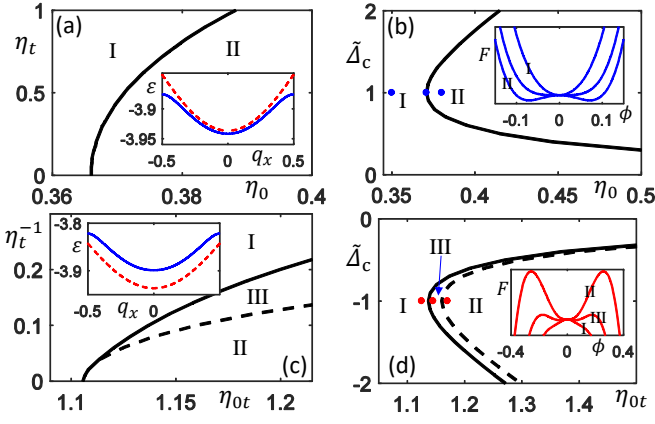


FIG. 3: (a) and (b) Phase diagrams for dominant intra-sideband coupling, with $\tilde{\Delta}_c = 1$ in (a) and $\eta_t = 0.5$ in (b). I (II) represents the normal (superradiant) phase. (c) and (d) Phase diagrams for dominant inter-sideband coupling, with $\tilde{\Delta}_c = -1$ in (c) and $\eta_t^{-1} = 0.1$ in (d), $\eta_{0t} = \eta_0 \eta_t$. III represents the hysteresis region. The insets in (a) and (c) show the s_0 -band dispersion in the normal (red dashed line) and superradiant phase (blue solid line). The three blue (red) dots in (b) [(d)] belong to different phases and they mark the points where the free energy curves are plotted in the inset. The parameters are $v_e = -6$, $\omega = 4.8$ and $\gamma = 2$ (with energy unit $E_R = \hbar^2 k_0^2 / 2m$), and atom-atom interaction is neglected.

terms $\propto e^{\pm i\omega t}$ can be dropped in Eq. (3). The steady state solution in the presence of cavity loss is determined by $\dot{\alpha} = 0$, yielding

$$\phi = 2\tilde{\Delta}_c \eta_0 \Theta_0 / (\tilde{\Delta}_c^2 + \gamma^2/4), \quad (4)$$

where $\phi \equiv \alpha + \alpha^*$, $\tilde{\Delta}_c = \Delta_c - u_0$ is the effective detuning with $u_0 = \frac{1}{T} \int_0^T dt u(t)$ a small constant, and $\Theta_0 = \frac{1}{T} \int_0^T dt \Theta(t)$ with $T = 2\pi/\omega$ the period. The shaking cavity field ϕ and atom density order Θ_0 are determined self-consistently through Eq. (4).

In the self-consistent determination, we replace $\frac{c^\dagger + c}{\sqrt{N_a}}$ in $\hat{V}_c(x, t)$ [Eq. (2)] by ϕ for the Floquet Hamiltonian $H_a(t)$ [Eq. (1)] and find Floquet quasi-energy bands and Floquet states for the BEC, from which the atom density order Θ can be calculated [65]. Θ in turn drives the cavity field ϕ through Eq. (3) as the atom feedback, yielding the self-adapted steady solution in Eq. (4). We find that solving the self-consistent equation Eq. (4) is equivalent to finding the extremum of the free energy density $F(\phi) = \langle \mathcal{H} \rangle / N_a$ (i.e., $\frac{\partial F}{\partial \phi} = 0$) [65]. Notice that $\phi = \Theta_0 = 0$ is always a trivial solution. Across the transition from normal to superradiant phases, the zero solution becomes unstable and ϕ , Θ_0 evolve from zero to finite values.

Results.—We focus on non-interacting BECs and discuss the interaction effects later. The numerically calculated phase diagrams and corresponding self-adapted Floquet bands with $\omega \gtrsim E_{sp} + |t_s| + |t_p|$ are shown in

Fig. 3. For a small η_t ($\lesssim 1$), \hat{V}_c is dominated by the time-independent term that couples s_0 and s_π bands, which would lower the energy of s_0 band [see the inset in Fig. 3(a)], indicating $\langle \hat{V}_c \rangle = -\eta_0 \phi \Theta_0 < 0$. According to Eq. (4), a non-trivial steady state solution exists only for blue effective detuning $\tilde{\Delta}_c > 0$ [Figs. 3(a) (b)]. The phase transition requires a stronger η_0 as η_t increases, indicating that the transition becomes harder due to the competition between inter- and intra-sideband couplings. As $\tilde{\Delta}_c$ decreases, the critical value of η_0 required for superradiance first decreases then increases and tends to infinity at $|\tilde{\Delta}_c| = 0$. This is because \hat{V}_c , which drives the atomic density order Θ_0 , is proportional to ϕ and approaches zero as $|\tilde{\Delta}_c| \rightarrow 0$ [see Eq. (4)]. We find that the solution is located at the minima of $F(\phi)$, which can be expanded as $F(\phi) = a_2 \phi^2 + a_4 \phi^4 + \dots$. $F(\phi)$ exhibits a continuous transition from a single minimum at $\phi = 0$ to double minima at $\phi \neq 0$ [see the inset in Fig. 3(b)], where a_2 and a_4 are both positive before the transition, and a_2 changes sign when the phase transition (second order) occurs.

For a large η_t ($\gg 1$), \hat{V}_c is dominated by the inter-band coupling between s_0 band and p_π band that has a lower energy than s_0 band, therefore atoms stays at the high-energy excited band and increasing the cavity field would rise the band energy [the inset in Fig. 3(c)] of the BEC, leading to $\langle \hat{V}_c \rangle = -\eta_0 \phi \Theta_0 > 0$. As a result, the non-trivial steady state solution exists only for red effective detuning $\tilde{\Delta}_c < 0$ [Figs. 3(c) (d)]. Surprisingly, the steady state solution is found at the maxima of $F(\phi)$ which exhibits a transition from a single maximum at $\phi = 0$ to double maxima at $\phi \neq 0$ [the inset in Fig. 3(d)] because of the non-equilibrium phase transition of the dynamical steady states which may not minimize the energy. Without Floquet sidebands, such superradiance at energy maximum for $\tilde{\Delta}_c < 0$ would not exist because atoms generally prefer staying in the lowest static band which can only couple with higher static bands.

Moreover, depending on the value of η_t , the transition can be either continuous (second order) or discontinuous with a hysteresis loop (first order) [Fig. 4(b)]. Such hysteresis originates from the interplay between intra-sideband and inter-sideband couplings, which induces a second-order coupling (similar to a two-photon Raman process) between s_0 and p_0 bands mediated by s_π and p_π bands (see Fig. 2(b)). Notice that the p_0 band is just below the s_0 band, therefore this second-order coupling rises the s_0 band by increasing a_4 . As a result, a_4 may change sign (from negative to positive) prior to a_2 changes sign (from negative to positive) when the second-order coupling is strong enough, leading to a multi-stability behavior where $F(\phi)$ exhibits three maxima simultaneously.

Hysteresis phenomena are related to strong nonlinearities [78], which are usually induced by strong atom-atom interactions [57, 60]. For example, the strong Ising interaction in the Dicke model can lead to a hysteresis loop

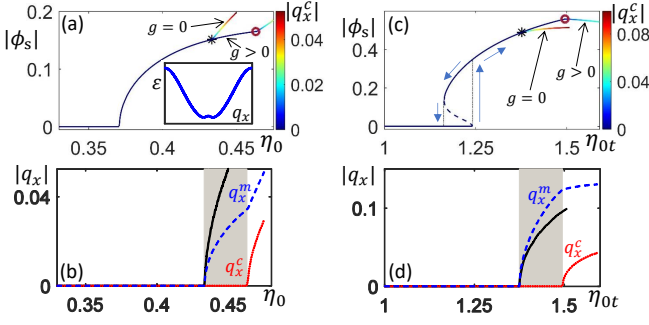


FIG. 4: (a) and (c) Superradiant order parameters and condensate momenta versus η_0 and η_{0t} . Stars and circles mark the transition points between zero and finite condensate momenta for $g = 0$ and $g > 0$, respectively. The inset of (a) shows the band structure for $|q_x^m| > 0$. A clear hysteresis loop appears in (c) with solid lines (dashed lines) corresponding to stable (unstable) steady-state solutions. (b) and (d) Difference between q_x^c (red dotted line) and q_x^m (blue dashed line) for $g > 0$. In the gray region, bosons are condensed into the local band maximum at $q_x = 0$. The black solid line shows $q_x^m = q_x^c$ for $g = 0$. (a) and (b) [(c) and (d)] correspond to dominant intra-sideband (inter-sideband) coupling with $\Delta_c = 1$, $\eta_t = 0.5$ and $g\bar{n} = 0.02$ ($\Delta_c = -1$, $\eta_t^{-1} = 0.15$ and $g\bar{n} = 0.1$). $\bar{n} = N_a/L$ is the average density with L the system size. Other parameters are the same as in Fig. 3.

of the superradiant phase transition [57–59]. However, the hysteresis effect in our system does not need atom-atom interaction at all, and has a completely different mechanism originating from the coupling between Floquet sidebands induced by the shaken cavity mode. Our study offers an excellent example and a realistic system for observing hysteresis effects without atom interactions.

As the superradiant field increases, the s_0 - p_0 band coupling would induce a transition of the Floquet band $\tilde{\varepsilon}_{s_0}(q_x)$ from a single minimum at $q_x = 0$ to doubly degenerate minima at $q_x \neq 0$ [see inset in Fig. 4(a)]. In our system, the s_0 - p_0 band coupling is a Raman-like coupling mediated by s_π and p_π , therefore such transition should be observed when the inter- and intra-sideband couplings coexist. We consider atom-atom interaction (tunable through Feshbach resonance [79]) that is weak and repulsive, therefore the interaction energy is always minimized when the system stays in a single momentum state. We assume that $\tilde{\varepsilon}_{s_0}(q_x)$ is minimized at $\pm q_x^m$. For negligibly weak interaction, the condensate momentum q_x^c would locate at one of the band minima (either $+q_x^m$ or $-q_x^m$) due to spontaneous symmetry breaking [80]. Such a transition in the BEC would also lead to a second order transition [stars in Figs. 4(a) (c)] of the shaking cavity field ϕ_s due to the back action.

As the atom-atom interaction increases (still weak enough such that the superradiant phase transition is not affected and the long-time behaviors (heating, atom loss, etc.) are not significant [22, 25, 81]), the phase transition of the BECs from $q_x^c = 0$ to $q_x^c \neq 0$ may be shifted be-

cause $q_x^c \neq \pm q_x^m$. q_x^c should be determined by minimizing $\tilde{\varepsilon}_{s_0}(q_x) + \tilde{\varepsilon}_{\text{int}}(q_x)$, with $\tilde{\varepsilon}_{\text{int}}(q_x)$ the momentum-dependent interaction energy,

$$\tilde{\varepsilon}_{\text{int}}(q_x) = \frac{1}{T} \int dt \int dx \frac{g}{2} |n_{s_0, q_x}(x, t)|^2. \quad (5)$$

Here g is the interaction constant and $n_{s_0, q_x}(x, t) = \langle \Psi^\dagger \Psi \rangle$ is the atom density. In our system, band mixing enhances spatial modulation of the density, and the interaction energy $\tilde{\varepsilon}_{\text{int}}(q_x)$ is minimized at $q_x = 0$ where the mixing is the smallest. As a result, q_x^c is smaller than q_x^m , and bosons may be condensed into the local maximum of the single-particle band at $q_x = 0$ [see Figs. 4(b) (d)]. The transition from $q_x^c = 0$ to $q_x^c \neq 0$ for $g > 0$ requires a stronger super-radiant field than the transition for $g = 0$ [see Figs. 4(a) (c)], and it also leads to a second order transition of ϕ_s which in turn leads to a transition in q_x^m .

Experimental consideration.—We consider a high-finesse (low-loss) cavity with $\gamma = 2E_R$ (with $E_R = \hbar^2 k_0^2 / 2m$ the recoil energy). Generally, atoms with a small mass are preferred to obtain a large E_R , thus a large γ , which makes the cavity easy to realize. For example, ^7Li (^{23}Na) atoms has a recoil energy $E_R \sim 40\text{kHz}$ (10kHz), corresponding to $\gamma = 80\text{kHz}$ (20kHz), which can be realized with current technique [65, 82]. The shaking frequency ω_0 is about several ten kHz for ^{23}Na and several hundred kHz for ^7Li (both are much smaller than the free spectral range $\sim\text{GHz}$), and such phase modulation can be implemented by PZT-driving mirrors or low-loss EOMs [65]. The system studied here only involves a change of introducing PZT-driving mirrors or inserting two EOMs into the setups used in the ETH and Hamburg laboratories [45, 49, 52, 53, 82], and thus should be feasible with current technology. Moreover, our model can also be implemented by combining a shaking external lattice and a periodic driving force (e.g., using a periodically modulated magnetic field gradient) [65].

Discussion.—We proposed a new type of Floquet physics where the parameter modulations are not only related to external driving, but also mutually coupled with system dynamics. As an example, we studied such Floquet dynamics of BECs in shaking optical lattices, which lead to interesting new phenomena including self-adapted shaking fields, Floquet bands and hysteresis effects. Such self-adapted Floquet physics may also arise in various other systems such as Rydberg-atom or molecule micromaser [83], ion-trap cavity [84] and circuit quantum electrodynamics (circuit QED) [85], etc. For example, in a circuit QED system, the electromagnetic field on the waveguide resonator can be periodically modulated by attaching superconducting quantum interference devices (SQUIDs) to the ends of the resonator, with the SQUIDs driving by external magnetic fluxes [86]. Such a modulated waveguide resonator can couple with su-

perconducting qubits (artificial atoms) and these qubits may also strongly couple with each other, where interesting self-adapted Floquet dynamics may emerge. Such self-adapted Floquet circuit QED may find important applications in quantum information processing and will be addressed in future works. Within the shaking lattice cavity system, interesting physics may also arise by considering strong atom-atom interaction (Bose-Hubbard model [52, 53]) or strong atom-single-photon coupling (limit cycles and chaos [87]), and superradiance of fermion gases (topological bands [88, 89]). In this spirit, our proposal opens up new possibilities for studying self-adapted Floquet physics in various systems, which may pave a way for engineering new exotic quantum matter.

Acknowledgements: We thank A. Hemmerich for helpful discussion. This work is supported by AFOSR (FA9550-16-1-0387), NSF (PHY-1505496), and ARO (W911NF-17-1-0128).

* Electronic address: chuanwei.zhang@utdallas.edu

- [1] N. H. Lindner, G. Refael, and V. Galitski, Floquet topological insulator in semiconductor quantum wells, *Nat. Phys.* **7**, 490–495 (2011).
- [2] Y. H. Wang, H. Steinberg, P. Jarillo-Herrero, and N. Gedik, Observation of floquet-bloch states on the surface of a topological insulator, *Science* **342**, 453–457 (2013).
- [3] U. De Giovannini, H. Hübener, and A. Rubio, Monitoring electron-photon dressing in wse₂, *Nano Lett.* **16**, 7993–7998 (2016).
- [4] J. Cayssol, B. Dóra, F. Simon, and R. Moessner, Floquet topological insulators, *Physica Status Solidi RRL* **7**, 101–108 (2013).
- [5] H. Hübener, M. A. Sentef, U. De Giovannini, A. F. Kemper, and A. Rubio, Creating stable floquet–weyl semimetals by laser-driving of 3d dirac materials, *Nat. Commun.* **8**, 13940 (2017).
- [6] N. Goldman and J. Dalibard, Periodically driven quantum systems: Effective hamiltonians and engineered gauge fields, *Phys. Rev. X* **4**, 031027 (2014).
- [7] M. Holthaus, Floquet engineering with quasienergy bands of periodically driven optical lattices, *J. Phys. B: At. Mol. Opt. Phys.* **49**, 013001 (2015).
- [8] A. Eckardt, Colloquium: Atomic quantum gases in periodically driven optical lattices, *Rev. Mod. Phys.* **89**, 011004 (2017).
- [9] T. Kitagawa, M. A. Broome, A. Fedrizzi, M. S. Rudner, E. Berg, I. Kassal, A. Aspuru-Guzik, E. Demler, and A. G. White, Observation of topologically protected bound states in photonic quantum walks, *Nat. Commun.* **3**, 882 (2012).
- [10] K. Fang, Z. Yu, and S. Fan, Realizing effective magnetic field for photons by controlling the phase of dynamic modulation, *Nat. Photon.* **6**, 782–787 (2012).
- [11] M. C. Rechtsman, J. M. Zeuner, Y. Plotnik, Y. Lumer, D. Podolsky, F. Dreisow, S. Nolte, M. Segev, and A. Szameit, Photonic floquet topological insulators, *Nature* **496**, 196–200 (2013).
- [12] K. Fang, Z. Yu, and S. Fan, Photonic aharonov-bohm effect based on dynamic modulation, *Phys. Rev. Lett.* **108**, 153901 (2012).
- [13] E. Li, B. J. Eggleton, K. Fang, and S. Fan, Photonic aharonov–bohm effect in photon–phonon interactions, *Nat. Commun.* **5**, 3225 (2014).
- [14] D. N. Basov, R. D. Averitt, and D. Hsieh, Towards properties on demand in quantum materials, *Nat. Mater.* **16**, 1077–1088 (2017).
- [15] D. H. Dunlap and V. M. Kenkre, Dynamic localization of a charged particle moving under the influence of an electric field, *Phys. Rev. B* **34**, 3625–3633 (1986).
- [16] V. V. Ivanov, A. Alberti, M. Schioppo, G. Ferrari, M. Artoni, M. L. Chiofalo, and G. M. Tino, Coherent delocalization of atomic wave packets in driven lattice potentials, *Phys. Rev. Lett.* **100**, 043602 (2008).
- [17] C. Sias, H. Lignier, Y. P. Singh, A. Zenesini, D. Ciampini, O. Morsch, and E. Arimondo, Observation of photon-assisted tunneling in optical lattices, *Phys. Rev. Lett.* **100**, 040404 (2008).
- [18] E. Haller, R. Hart, M. J. Mark, J. G. Danzl, L. Reichsöllner, and H.-C. Nägerl, Inducing transport in a dissipation-free lattice with super bloch oscillations, *Phys. Rev. Lett.* **104**, 200403 (2010).
- [19] A. Alberti, V. V. Ivanov, G. M. Tino, and G. Ferrari, Engineering the quantum transport of atomic wavefunctions over macroscopic distances, *Nat. Phys.* **5**, 547–550 (2009).
- [20] N. Gemelke, E. Sarajlic, Y. Bidel, S. Hong, and S. Chu, Parametric amplification of matter waves in periodically translated optical lattices, *Phys. Rev. Lett.* **95**, 170404 (2005).
- [21] W. S. Bakr, P. M. Preiss, M. E. Tai, R. Ma, J. Simon, and M. Greiner, Orbital excitation blockade and algorithmic cooling in quantum gases, *Nature* **480**, 500–503 (2011).
- [22] C. V. Parker, L.-C. Ha, and C. Chin, Direct observation of effective ferromagnetic domains of cold atoms in a shaken optical lattice, *Nat. Phys.* **9**, 769–774 (2013).
- [23] L.-C. Ha, L. W. Clark, C. V. Parker, B. M. Anderson, and C. Chin, Roton-maxon excitation spectrum of bose condensates in a shaken optical lattice, *Phys. Rev. Lett.* **114**, 055301 (2015).
- [24] Z. Zheng, C. Qu, X. Zou, and C. Zhang, Fulde-ferrell superfluids without spin imbalance in driven optical lattices, *Phys. Rev. Lett.* **116**, 120403 (2016).
- [25] M. A. Khamsehchi, C. Qu, M. E. Mossman, C. Zhang, and P. Engels, Spin-momentum coupled bose-einstein condensates with lattice band pseudospins, *Nat. Commun.* **7**, 10867 (2016).
- [26] A. S. Sørensen, E. Demler, and M. D. Lukin, Fractional quantum hall states of atoms in optical lattices, *Phys. Rev. Lett.* **94**, 086803 (2005).
- [27] T. Kitagawa, E. Berg, M. Rudner, and E. Demler, Topological characterization of periodically driven quantum systems, *Phys. Rev. B* **82**, 235114 (2010).
- [28] M. Aidelsburger, M. Atala, M. Lohse, J. T. Barreiro, B. Paredes, and I. Bloch, Realization of the hofstadter hamiltonian with ultracold atoms in optical lattices, *Phys. Rev. Lett.* **111**, 185301 (2013).
- [29] M. Aidelsburger, M. Atala, S. Nascimbène, S. Trotzky, Y.-A. Chen, and I. Bloch, Experimental realization of strong effective magnetic fields in an optical lattice, *Phys. Rev. Lett.* **107**, 255301 (2011).

- [30] J. Struck, C. Ölschläger, M. Weinberg, P. Hauke, J. Simonet, A. Eckardt, M. Lewenstein, K. Sengstock, and P. Windpassinger, Tunable gauge potential for neutral and spinless particles in driven optical lattices, *Phys. Rev. Lett.* **108**, 225304 (2012).
- [31] J. Struck, M. Weinberg, C. Ölschläger, P. Windpassinger, J. Simonet, K. Sengstock, R. Höppner, P. Hauke, A. Eckardt, M. Lewenstein, and L. Mathey, Engineering ising-xy spin-models in a triangular lattice using tunable artificial gauge fields, *Nat. Phys.* **9**, 738–743 (2013).
- [32] H. Miyake, G. A. Siviloglou, C. J. Kennedy, W. C. Burton, and W. Ketterle, Realizing the harper hamiltonian with laser-assisted tunneling in optical lattices, *Phys. Rev. Lett.* **111**, 185302 (2013).
- [33] M. Atala, M. Aidelsburger, M. Lohse, J. T. Barreiro, B. Paredes, and I. Bloch, Observation of chiral currents with ultracold atoms in bosonic ladders, *Nat. Phys.* **10**, 588–593 (2014).
- [34] C. J. Kennedy, W. C. Burton, W. C. Chung, and W. Ketterle, Observation of bose-einstein condensation in a strong synthetic magnetic field, *Nat. Phys.* **11**, 859–864 (2015).
- [35] M. E. Tai, A. Lukin, M. Rispoli, R. Schittko, T. Menke, D. Borgnia, P. M. Preiss, F. Grusdt, A. M. Kaufman, and M. Greiner, Microscopy of the interacting harper-hofstadter model in the two-body limit, *Nature* **546**, 519–523 (2017).
- [36] G. Jotzu, M. Messer, R. Desbuquois, M. Lebrat, T. Uehlinger, D. Greif, and T. Esslinger, Experimental realization of the topological haldane model with ultracold fermions, *Nature* **515**, 237–240 (2014).
- [37] M. Aidelsburger, M. Lohse, C. Schweizer, M. Atala, J. T. Barreiro, S. Nascimbene, N. R. Cooper, I. Bloch, and N. Goldman, Measuring the chern number of hofstadter bands with ultracold bosonic atoms, *Nat. Phys.* **11**, 162–166 (2015).
- [38] A. Eckardt, C. Weiss, and M. Holthaus, Superfluid-insulator transition in a periodically driven optical lattice, *Phys. Rev. Lett.* **95**, 260404 (2005).
- [39] H. Lignier, C. Sias, D. Ciampini, Y. Singh, A. Zenesini, O. Morsch, and E. Arimondo, Dynamical control of matter-wave tunneling in periodic potentials, *Phys. Rev. Lett.* **99**, 220403 (2007).
- [40] A. Zenesini, H. Lignier, D. Ciampini, O. Morsch, and E. Arimondo, Coherent control of dressed matter waves, *Phys. Rev. Lett.* **102**, 100403 (2009).
- [41] J. Struck, C. Ölschläger, R. L. Targat, P. Soltan-Panahi, A. Eckardt, M. Lewenstein, P. Windpassinger, and K. Sengstock, Quantum simulation of frustrated classical magnetism in triangular optical lattices, *Science* **333**, 996–999 (2011).
- [42] H. Walther, B. T. H. Varcoe, B.-G. Englert, and T. Becker, Cavity quantum electrodynamics, *Rep. Prog. Phys.* **69**, 1325 (2006).
- [43] A. T. Black, H. W. Chan, and V. Vuletić, Observation of collective friction forces due to spatial self-organization of atoms: From rayleigh to bragg scattering, *Phys. Rev. Lett.* **91**, 203001 (2003).
- [44] S. Slama, S. Bux, G. Krenz, C. Zimmermann, and Ph. W. Courteille, Superradiant rayleigh scattering and collective atomic recoil lasing in a ring cavity, *Phys. Rev. Lett.* **98**, 053603 (2007).
- [45] K. Baumann, C. Guerlin, F. Brennecke, and T. Esslinger, Dicke quantum phase transition with a superfluid gas in an optical cavity, *Nature* **464**, 1301–1306 (2010).
- [46] K. Baumann, R. Mottl, F. Brennecke, and T. Esslinger, Exploring symmetry breaking at the dicke quantum phase transition, *Phys. Rev. Lett.* **107**, 140402 (2011).
- [47] K. J. Arnold, M. P. Baden, and M. D. Barrett, Self-organization threshold scaling for thermal atoms coupled to a cavity, *Phys. Rev. Lett.* **109**, 153002 (2012).
- [48] H. Ritsch, P. Domokos, F. Brennecke, and T. Esslinger, Cold atoms in cavity-generated dynamical optical potentials, *Rev. Mod. Phys.* **85**, 553–601 (2013).
- [49] H. Keßler, J. Klinder, M. Wolke, and A. Hemmerich, Steering matter wave superradiance with an ultranarrow-band optical cavity, *Phys. Rev. Lett.* **113**, 070404 (2014).
- [50] M. Reza Bakhtiari, A. Hemmerich, H. Ritsch, and M. Thorwart, Nonequilibrium phase transition of interacting bosons in an intra-cavity optical lattice, *Phys. Rev. Lett.* **114**, 123601 (2015).
- [51] S. Gopalakrishnan, B. L. Lev, and P. M. Goldbart, Emergent crystallinity and frustration with bose-einstein condensates in multimode cavities, *Nat. Phys.* **5**, 845–850 (2009).
- [52] J. Klinder, H. Keßler, M. Reza Bakhtiari, M. Thorwart, and A. Hemmerich, Observation of a superradiant mott insulator in the dicke-hubbard model, *Phys. Rev. Lett.* **115**, 230403 (2015).
- [53] R. Landig, L. Hruby, N. Dogra, M. Landini, R. Mottl, T. Donner, and T. Esslinger, Quantum phases from competing short-and long-range interactions in an optical lattice, *Nature* **532**, 476–479 (2016).
- [54] B. W. Shore and P. L. Knight, The jaynes-cummings model, *J. Mod. Opt.* **40**, 1195–1238 (1993).
- [55] R. H. Dicke, Coherence in spontaneous radiation processes, *Phys. Rev.* **93**, 99–110 (1954).
- [56] D. Nagy, G. Kónya, G. Szirmai, and P. Domokos, Dicke-model phase transition in the quantum motion of a bose-einstein condensate in an optical cavity, *Phys. Rev. Lett.* **104**, 130401 (2010).
- [57] C. F. Lee and N. F. Johnson, First-order superradiant phase transitions in a multiqubit cavity system, *Phys. Rev. Lett.* **93**, 083001 (2004).
- [58] S. Gammelmark and K. Mølmer, Phase transitions and heisenberg limited metrology in an ising chain interacting with a single-mode cavity field, *New J. Phys.* **13**, 053035 (2011).
- [59] X.-W. Luo, Y.-N. Zhang, X. Zhou, G.-C. Guo, and Z.-W. Zhou, Dynamic phase transitions of a driven ising chain in a dissipative cavity, *Phys. Rev. A* **94**, 053809 (2016).
- [60] S. Eckel, J. G. Lee, F. Jendrzejewski, N. Murray, C. W. Clark, C. J. Lobb, W. D. Phillips, M. Edwards, and G. K. Campbell, Hysteresis in a quantized superfluid ‘atomtronic’ circuit, *Nature (London)* **506**, 200–203 (2014).
- [61] C. Hamner, C. Qu, Y. Zhang, J. Chang, M. Gong, C. Zhang, and P. Engels, Dicke-type phase transition in a spin-orbit-coupled Bose-Einstein condensate, *Nat. Commun.* **5**, 4023 (2014).
- [62] A. Trenkwalder, G. Spagnolli, G. Semeghini, S. Coop, M. Landini, P. Castilho, L. Pezze, G. Modugno, M. Inguscio, A. Smerzi, and M. Fattori, Quantum phase transitions with parity-symmetry breaking and hysteresis, *Nat. Phys.* **12**, 826–829 (2016).
- [63] A. Yariv and P. Yeh, *Photonics: Optical Electronics in Modern Communications* (Oxford University Press, New

- York, NY, 2007).
- [64] D. Goldovsky, V. Jouravsky, and A. Peer, Simple and robust phase-locking of optical cavities with > 200 KHz servo-bandwidth using a piezo-actuated mirror mounted in soft materials, *Opt. Exp.* **24**, 28239 (2016).
 - [65] See Supplemental Material for more details about the cavity-assisted potential, the Floquet bands and energy density, the stability analysis and the experimental consideration, which includes Refs. [66–77].
 - [66] R. Gehr, J. Volz, G. Dubois, T. Steinmetz, Y. Colombe, B. L. Lev, R. Long, J. Esteve, and J. Reichel, Cavity-based single atom preparation and high-fidelity hyperfine state readout, *Phys. Rev. Lett.* **104**, 203602 (2010).
 - [67] M. J. Bhaseen, J. Mayoh, B. D. Simons, and J. Keeling, Dynamics of nonequilibrium dicke models, *Phys. Rev. A* **85**, 013817 (2012).
 - [68] D. Nagy, G. Szirmai, and P. Domokos, Critical exponent of a quantum-noise-driven phase transition: The open-system dicke model, *Phys. Rev. A* **84**, 043637 (2011).
 - [69] T. Nakamura, S. Tani, I. Ito, and Y. Kobayashi, Beyond 500-kHz Bandwidth Piezo-Electric Transducers For GHz-Comb Applications, 2017 European Quantum Electronics Conference, ED.P_4 (2017).
 - [70] R. J. Jones, K. D. Moll, M. J. Thorpe, and J. Ye, Phase-Coherent Frequency Combs in the Vacuum Ultraviolet via High-Harmonic Generation inside a Femtosecond Enhancement Cavity, *Phys. Rev. Lett.* **94**, 193201 (2005).
 - [71] A. M. Warrier, J. Lin, H. M. Pask, R. P. Mildren, D. W. Coutts, and D. J. Spence, Highly efficient picosecond diamond Raman laser at 1240 and 1485 nm, *Opt. Exp.* **22**, 3325 (2014).
 - [72] H. K. Raut, V. A. Ganesh, A. S. Nair, and S. Ramakrishna, Anti-reflective coatings: A critical, in-depth review, *Energy Environ. Sci.* **4**, 3779–3804 (2011).
 - [73] M. Roth, N. Angert, M. Tseitlin, and A. Alexandrovski, On the optical quality of KTP crystals for nonlinear optical and electro-optic applications, *Opt. Mater.* **16**, 131 (2001).
 - [74] M. Leidinger, K. Buse, and I. Breunig, Highly sensitive absorption measurements in lithium niobate using whispering gallery resonators, *Proc. SPIE* **9347**, 93471D (2015).
 - [75] N. Waasem, S. Fieberg, J. Hauser, G. Gomes, D. Haertle, F. Kühnemann, and K. Buse, Photoacoustic absorption spectrometer for highly transparent dielectrics with parts-per-million sensitivity, *Rev. Sci. Instrum.* **84**, 023109 (2013).
 - [76] A. Yariv and P. Yeh, *Optical Waves in Crystals, Propagation and Control of Laser Radiation* (John Wiley and Sons, New York, 1984).
 - [77] X. Luo, L. Wu, J. Chen, Q. Guan, K. Gao, Z.-F. Xu, L. You, and R. Wang, Tunable atomic spin-orbit coupling synthesized with a modulating gradient magnetic field, *Sci. Rep.* **6**, 18983, (2016).
 - [78] P. G. Drazin, *Nonlinear systems* (Cambridge University Press, Cambridge, England, 1992).
 - [79] C. Chin, R. Grimm, P. Julienne, and E. Tiesinga, Feshbach resonances in ultracold gases, *Rev. Mod. Phys.* **82**, 1225–1286 (2010).
 - [80] W. Zheng, B. Liu, J. Miao, C. Chin, and H. Zhai, Strong interaction effects and criticality of bosons in shaken optical lattices, *Phys. Rev. Lett.* **113**, 155303 (2014).
 - [81] T. Bilitewski, and N. R. Cooper, Scattering theory for Floquet-Bloch states, *Phys. Rev. A* **91**, 033601 (2015).
 - [82] B. Nagorny, Th. Elsässer, and A. Hemmerich, Collective atomic motion in an optical lattice formed inside a high finesse cavity, *Phys. Rev. Lett.* **91**, 153003 (2003).
 - [83] H. Walther, Experiments on cavity quantum electrodynamics, *Phys. Rep.* **219**, 263 (1992).
 - [84] M. Keller, B. Lange, K. Hayasaka, W. Lange, and H. Walther, Continuous generation of single photons with controlled waveform in an ion-trap cavity system, *Nature* **431**, 1075 (2004).
 - [85] A. Wallraff, D. I. Schuster, A. Blais, L. Frunzio, R.-S. Huang, J. Majer, S. Kumar, S. M. Girvin, and R. J. Schoelkopf, Strong coupling of a single photon to a superconducting qubit using circuit quantum electrodynamics, *Nature* **431**, 162 (2004).
 - [86] C. M. Wilson, G. Johansson, A. Pourkabirian, M. Simoen, J. R. Johansson, T. Duty, F. Nori, and P. Delsing, Observation of the dynamical Casimir effect in a superconducting circuit, *Nature* **479**, 376 (2011).
 - [87] F. Piazza and H. Ritsch, Self-ordered limit cycles, chaos, and phase slippage with a superfluid inside an optical resonator, *Phys. Rev. Lett.* **115**, 163601 (2015).
 - [88] Y. Chen, Z. Yu, and H. Zhai, Superradiance of degenerate Fermi gases in a cavity, *Phys. Rev. Lett.* **112**, 143004 (2014).
 - [89] J.-S. Pan, X.-J. Liu, W. Zhang, W. Yi, and G.-C. Guo, Topological superradiant states in a degenerate fermi gas, *Phys. Rev. Lett.* **115**, 045303 (2015).

Supplementary Materials

Cavity-assisted shaking lattices and background lattices

In this section, we give the detailed derivation of the cavity-assisted shaking potential of Eq. (2) in the main text, and discuss the possible realizations of the background lattice.

The shaking cavity mode can be expanded using the Bessel function expansion $e^{if \cos \omega_0 t} = \sum_n i^n J_n(f) e^{in\omega_0 t}$,

$$\begin{aligned} \cos[k_0 x + \varphi_0 + f \cos(\omega_0 t)] &= \cos(k_0 x) [J_0(f) \cos(\varphi_0) + 2J_1(f) \sin(\varphi_0) \cos(\omega_0 t) + 2 \cos(\varphi_0) J_2(f) \cos(2\omega_0 t)] \\ &\quad + \sin(k_0 x) [J_0(f) \sin(\varphi_0) + 2J_1(f) \cos(\varphi_0) \cos(\omega_0 t) + 2 \sin(\varphi_0) J_2(f) \cos(2\omega_0 t)] \\ &\quad + \dots \end{aligned} \quad (S1)$$

We consider that only the static s band and two-phonon-dressed p band are near resonance ($2\omega_0 \sim E_{sp}$), and the

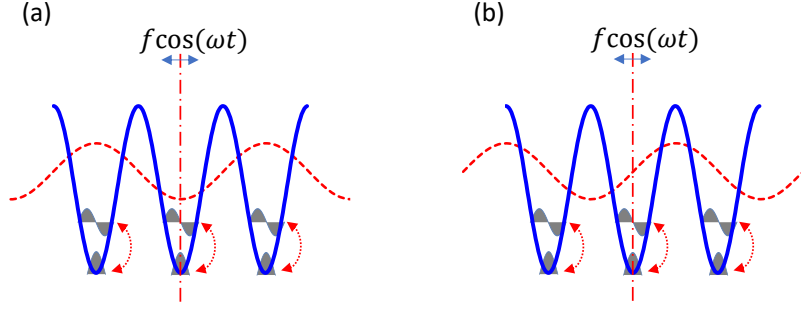


FIG. S1: Parity of the cavity field (red dashed curve) with respect to the back ground lattice (blue solid curve) for $\varphi_0 = 0$ in (a) and $\varphi_0 = \frac{\pi}{2}$ in (b).

static lattice potential V_{ext} is much stronger than the shaking cavity field. Due to the parity of the Wannier functions, $\sin(k_0 x)$ only induces inter-band couplings between s and p bands, while $\cos(k_0 x)$ only induces intra-band couplings. With proper choice of the parameters f , φ_0 and ω_0 , the expansion can be simplified by omitting small and far-off-resonance terms

$$\cos[k_0 x + \varphi_0 + f \cos(\omega_0 t)] \simeq J_0(f) \cos(\varphi_0) [\cos(k_0 x) + 4\eta_t \sin(k_0 x) \cos(\omega t)], \quad (\text{S2})$$

with $\eta_t = \frac{J_2(f)}{2J_0(f)} \tan(\varphi_0)$ and $\omega \equiv 2\omega_0$. Therefore, we obtain Eq. (2) in the main text

$$\hat{V}_c = -\eta_0 \frac{c^\dagger + c}{\sqrt{N_a}} [\cos(k_0 x) + 4\eta_t \cos(\omega t) \sin(k_0 x)]. \quad (\text{S3})$$

The ratio η_t between inter-sideband and intra-sideband couplings can be tuned through f and φ_0 . For $\varphi_0 = 0$, we have $\eta_0 = \eta J_0(f)$ and $\eta_0 \eta_t = 0$, corresponding to dominant intra-sideband coupling. While for $\varphi_0 = \frac{\pi}{2}$, we have $\eta_0 = 0$ and $\eta_0 \eta_t = \eta \frac{J_2(f)}{2}$, corresponding to dominant inter-sideband coupling. These properties can be understood from the parity of the cavity field with respect to the background lattice sites. Fig. S1(a) shows the cavity field for $\varphi_0 = 0$, where the static part of the cavity field is even with respect to the background lattice site, thus induces strong intra-sideband couplings due to the parity of the Wannier functions. While Fig. S1(b) shows the cavity field for $\varphi_0 = \frac{\pi}{2}$, where the static part of the cavity field is odd with respect to the background lattice site, and cannot induce intra-sideband couplings. With similar arguments, the shaking part, thus the inter-sideband coupling, is dominant for $\varphi_0 = \frac{\pi}{2}$.

The above discussion can be generalized to the case with resonance coupling between different side-bands. For example, we may consider the resonance coupling between s band and one-phonon-dressed d band $\omega_0 \sim E_{sd}$. Note that the coupling between s and d band is induced by $\cos(k_0 x)$, thus the shaken cavity mode can be simplified as

$$\cos[k_0 x + \varphi_0 + f \cos(\omega_0 t)] \simeq J_0(f) \cos(\varphi_0) \cos(k_0 x) [1 + 4\eta'_t \cos(\omega_0 t)], \quad (\text{S4})$$

with $\eta'_t = \frac{J_1(f)}{2J_0(f)} \tan(\varphi_0)$, which can be tuned through f and φ_0 .

The background lattice potential $V_{\text{ext}}(x)$ can be realized by additional lasers feeding into the cavity from the transverse side with a tilt angle θ and wavenumber $k_0/\cos(\theta)$ [1, 2]. Alternatively, $V_{\text{ext}}(x)$ can be realized by longitudinally pumping the $\hat{\mathbf{y}}$ -polarized cavity mode whose resonance frequency is far detuned from the $\hat{\mathbf{z}}$ -polarized mode (so we may treat them independently) [2–4] (in this case, one should use the EOMs to shake the cavity mode and the EOMs should only modify the optical path length of the $\hat{\mathbf{z}}$ -polarized mode [5]).

Floquet bands and states for the atomic system

Under mean-field approach, we replace operator $(c^\dagger + c)/\sqrt{N_a}$ in $\hat{V}_c(x, t)$ by its mean value ϕ , the Hamiltonian of the atomic system can be written as

$$\mathcal{H}_a(\phi, t) = \int dx \Psi^\dagger(x) \left[-\frac{\partial_x^2}{2m} + V_{\text{ext}}(x) + V_c \right] \Psi(x), \quad (\text{S5})$$

with $V_c = -\eta_0\phi[\cos(k_0x) + 4\eta_t \sin(k_0x) \cos(\omega t)]$. This Hamiltonian contains no photon operators, and is a typical Hamiltonian for ultracold atoms in shaking lattices which can be solved following the standard procedure. *In this section*, we show how to obtain the Floquet eigenstates and bands of the atomic system for a given ϕ , from which we can calculate the atomic density order Θ_0 and obtain the steady state solution self-consistently [see Eq. (4) in the main text].

We consider a deep external lattice $V_{\text{ext}}(x) = v_e \cos^2(k_0x)$ and a weak cavity field ϕ . The time independent part $-\frac{\partial_x^2}{2m} + V_{\text{ext}}(x)$ leads to a static band structure, and V_c as a perturbation drives the resonance coupling between s and p bands. Here we will focus on the dominant effects of the Floquet coupling and project the system onto the subspace spanned by the bands near resonance. For a deep background lattice $V_{\text{ext}}(x)$, we adopt the tight-binding approach and expand the wave function in the Wannier basis of the s and p bands $\Psi(x, t) = \sum_{\lambda,j} a_{\lambda,j}(t) W_{\lambda,j}(x)$ with site index j and band index $\lambda = s, p$. The Hamiltonian is

$$\mathcal{H}_a(t) = \sum_{\lambda,j} \left[E_{\lambda} a_{\lambda,j}^{\dagger} a_{\lambda,j} + t_{\lambda} (a_{\lambda,j+1}^{\dagger} a_{\lambda,j} + h.c.) \right] + \sum_{\lambda,j;\lambda',j'} \Omega_{\lambda,\lambda'}^{j,j'}(t) a_{\lambda',j'}^{\dagger} a_{\lambda,j} \quad (\text{S6})$$

with $\Omega_{\lambda,\lambda'}^{j,j'}(t) = \int dx W_{\lambda',j'}^*(x) V_c(x, t) W_{\lambda,j}(x)$ that drives the resonance coupling between s and p bands. The cavity field would hardly affect the tunnelings between neighbor sites for a deep background lattice, so we have $\Omega_{\lambda,\lambda'}^{j,j'} \sim 0$ for $j \neq j'$.

In the rotating frame with unitary transformation $U = \exp(-i \sum_j \omega a_{p,j}^{\dagger} a_{p,j} t)$, the Hamiltonian can be written as

$$\mathcal{H}_a(t) = \sum_j \Delta_p a_{p,j}^{\dagger} a_{p,j} + \sum_{\lambda,j} \left[t_{\lambda} (a_{\lambda,j+1}^{\dagger} a_{\lambda,j} + h.c.) + \Omega_{\lambda}^j(t) a_{\lambda,j}^{\dagger} a_{\lambda,j} \right] + \sum_j \left[e^{-i\omega t} \Omega_{s,p}^j(t) a_{s,j}^{\dagger} a_{p,j} + h.c. \right] + N_a E_s, \quad (\text{S7})$$

where $\Omega_{\lambda}^j(t) = \Omega_{\lambda,\lambda}^j(t) = \int dx W_{\lambda,j}^*(x) V_c(x, t) W_{\lambda,j}(x) = -\eta_0\phi \int dx W_{\lambda,j}^*(x) \cos(k_0x) W_{\lambda,j}(x)$, and $\Omega_{s,p}^j(t) = \Omega_{s,p}^j(t) = \int dx W_{s,j}^*(x) V_c(x, t) W_{p,j}(x) = -4\eta_0\eta_t\phi \cos(\omega t) \int dx W_{s,j}^*(x) \sin(k_0x) W_{p,j}(x)$. $\Delta_p = E_p - E_s - \omega$, and $N_a E_s$ is a constant. For a weak cavity field with $\Omega_{\lambda,\lambda'}^{j,j'} \ll \omega$, we drop the far-off-resonance terms and obtain the effective time-independent Hamiltonian as (to the leading order)

$$\bar{\mathcal{H}}_a = \frac{1}{T} \int dt \mathcal{H}_a(t) = \sum_j \Delta_p a_{p,j}^{\dagger} a_{p,j} + \sum_{\lambda,j} \left[t_{\lambda} (a_{\lambda,j+1}^{\dagger} a_{\lambda,j} + h.c.) + \Omega_{\lambda}^j a_{\lambda,j}^{\dagger} a_{\lambda,j} \right] + \sum_j \left[\Omega_{s,p}^j a_{s,j}^{\dagger} a_{p,j} + h.c. \right] \quad (\text{S8})$$

with $\Omega_{\lambda}^j = -\eta_0\phi \int dx W_{\lambda,j}^*(x) \cos(k_0x) W_{\lambda,j}(x)$ and $\Omega_{s,p}^j = -2\eta_0\eta_t\phi \int dx W_{s,j}^*(x) \sin(k_0x) W_{p,j}(x)$.

Notice that $\cos(k_0x)$ and $\sin(k_0x)$ have a spatial period which is twice of that for the background potential $V_{\text{ext}}(x)$, thus we have $\Omega_{\lambda}^j = (-1)^j \Omega_{\lambda}^{j=0}$ and $\Omega_{s,p}^j = (-1)^j \Omega_{s,p}^{j=0}$. In the Fourier space (i.e., the Bloch basis), $a_{\lambda,q_x} \propto \sum_j e^{iq_x j b} a_{\lambda,j}$ with $q_x \in [-k_0, k_0]$ and $b = \frac{\pi}{k_0}$ the lattice constant, we have

$$\bar{\mathcal{H}}_a = \sum_{\lambda,q_x} \left[\bar{\varepsilon}_{\lambda}(q_x) a_{\lambda,q_x}^{\dagger} a_{\lambda,q_x} + \Omega_{\lambda}(q_x) a_{\lambda,q_x}^{\dagger} a_{\lambda,q_x+k_0} \right] + \sum_{q_x} \left[\Omega_{s,p}(q_x) a_{s,q_x}^{\dagger} a_{p,q_x+k_0} + \Omega_{p,s}(q_x) a_{p,q_x}^{\dagger} a_{s,q_x+k_0} \right], \quad (\text{S9})$$

with $\bar{\varepsilon}_s(q_x) = t_s \cos(q_x b)$, $\bar{\varepsilon}_p(q_x) = \Delta_p + t_p \cos(q_x b)$, $\Omega_{\lambda}(q_x) = \Omega_{\lambda}^{j=0}$ and $\Omega_{s,p}(q_x) = \Omega_{p,s}(q_x) = \Omega_{s,p}^{j=0}$. Since each unit cell now contains two sites, the Brillouin zone (BZ) reduces in half and becomes $q_x \in [-k_0/2, k_0/2]$. Each band λ is split into two bands λ_0, λ_{π} , with $a_{\lambda_0}(q_x) = a_{\lambda}(q_x)$ and $a_{\lambda_{\pi}}(q_x) = a_{\lambda}(q_x + k_0)$. The Hamiltonian can be written as

$$\bar{\mathcal{H}}_a = (a_{p_{\pi}}^{\dagger}, a_{p_0}^{\dagger}, a_{s_0}^{\dagger}, a_{s_{\pi}}^{\dagger}) \bar{H}_a (a_{p_{\pi}}, a_{p_0}, a_{s_0}, a_{s_{\pi}})^T, \quad (\text{S10})$$

with

$$\bar{H}_a = \begin{pmatrix} \bar{\varepsilon}_{p_{\pi}}(q_x) & \Omega_p(q_x) & \Omega_{s,p}(q_x) & 0 \\ \Omega_p^*(q_x) & \bar{\varepsilon}_{p_0}(q_x) & 0 & \Omega_{p,s}^*(q_x) \\ \Omega_{s,p}^*(q_x) & 0 & \bar{\varepsilon}_{s_0}(q_x) & \Omega_s(q_x) \\ 0 & \Omega_{p,s}(q_x) & \Omega_s(q_x) & \bar{\varepsilon}_{s_{\pi}}(q_x) \end{pmatrix}. \quad (\text{S11})$$

Based on the time-independent Hamiltonian, we can obtain the Floquet s_0 band (i.e. the third band of $\bar{\mathcal{H}}_a$) with $\bar{\mathcal{H}}_a |s_0, q_x\rangle = \bar{\varepsilon}_{s_0}(q_x) |s_0, q_x\rangle$ and corresponding condensate atomic density $n_{s_0,q_x}(x, t) = \langle \Psi^{\dagger}(x, t) \Psi(x, t) \rangle = \langle s_0, q_x | U \Psi^{\dagger}(x, t) \Psi(x, t) U^{\dagger} | s_0, q_x \rangle$, which can be used to calculate the atomic density order Θ_0 . In our numerical

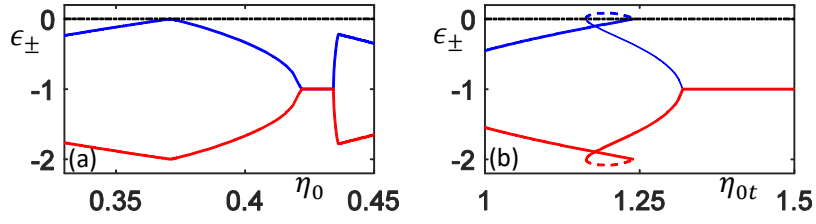


FIG. S2: Stability coefficients (blue and red solid lines) as a function of the coupling strength for $g = 0$, with black dash-dotted line representing the zero axis. (a) corresponds to dominant intra-sideband coupling with $\Delta_c = 1$ and $\eta_t = 0.5$. (b) corresponds to dominant inter-sideband coupling with $\Delta_c = -1$ and $\eta_t^{-1} = 0.15$. A clear hysteresis loop appears in (b) with solid lines (dashed lines) corresponding to stable (unstable) steady state solutions. Other parameters are the same as in Fig. 4(c) in the main text.

simulation, all matrix elements in \bar{H}_a are calculated directly in the Bloch basis, where the effects of small long-range tunnelings (e.g., $\Omega_{\lambda, \lambda'}^{j, j'}$ for $j \neq j'$) are also included. We emphasize here that our system is different from a system with shaking external lattices (which can not freely evolve) and static cavity fields, where the proposed self-adapted Floquet dynamics and the hysteresis phenomena would not exist due to the absence of cavity-assisted Floquet sideband couplings.

Energy density and self-consistent equation

In this section, we show that solving the self-consistent equation is equivalent to finding the extremum of the energy density.

The total Hamiltonian of the system is

$$\mathcal{H} = \tilde{\Delta}_c c^\dagger c + \int dx \Psi^\dagger(x) \left[-\frac{\partial_x^2}{2m} + V_{\text{ext}}(x) + \hat{V}_c(x, t) \right] \Psi(x), \quad (\text{S12})$$

with $\tilde{\Delta}_c = \Delta_c - u$. For a deep external potential $V_{\text{ext}}(x)$, atoms are well localized near its minima, therefore, the atom induced detuning becomes $u = \frac{g_0^2}{\Delta_c} \int dx \Psi^\dagger \Psi \cos^2(k_0 x + \varphi) \simeq \frac{g_0^2 N_a}{\Delta_c} \cos^2(\varphi)$, which is small and independent of the cavity field. Under the mean-field approach, the coupling term between atoms and the cavity field can be written as [6]

$$\begin{aligned} \int dx \Psi^\dagger(x) \hat{V}_c(x, t) \Psi(x) &= -\eta_0 \frac{c^\dagger + c}{\sqrt{N_a}} \int dx \Psi^\dagger(x) \Psi(x) [\cos(k_0 x) + 2\eta_t (e^{i\omega t} + e^{-i\omega t}) \sin(k_0 x)] \\ &= -\eta_0 \frac{c^\dagger + c}{\sqrt{N_a}} \int dx \langle \Psi^\dagger(x) \Psi(x) \rangle [\cos(k_0 x) + 2\eta_t (e^{i\omega t} + e^{-i\omega t}) \sin(k_0 x)] \\ &\quad - \eta_0 \langle \frac{c^\dagger + c}{\sqrt{N_a}} \rangle \int dx \Psi^\dagger(x) \Psi(x) [\cos(k_0 x) + 2\eta_t (e^{i\omega t} + e^{-i\omega t}) \sin(k_0 x)] \\ &\quad + \eta_0 \langle \frac{c^\dagger + c}{\sqrt{N_a}} \rangle \int dx \langle \Psi^\dagger(x) \Psi(x) \rangle [\cos(k_0 x) + 2\eta_t (e^{i\omega t} + e^{-i\omega t}) \sin(k_0 x)] \\ &= -\eta_0 \Theta(t) \sqrt{N_a} (c^\dagger + c) + \eta_0 \Theta(t) N_a \phi - \int dx \Psi^\dagger(x) V_c \Psi(x). \end{aligned} \quad (\text{S13})$$

Thus the total Hamiltonian can be written as

$$\mathcal{H} = \tilde{\Delta}_c c^\dagger c - \eta_0 \Theta(t) \sqrt{N_a} (c^\dagger + c) + \eta_0 \Theta(t) N_a \phi + \mathcal{H}_a(t). \quad (\text{S14})$$

with $\mathcal{H}_a(t)$ given by Eq. (S5).

We define the free energy F as the total energy density

$$F = \frac{1}{N_a} \langle \mathcal{H} \rangle. \quad (\text{S15})$$

After dropping the far-off resonance terms, we obtain $F = \tilde{\Delta}_c \alpha^* \alpha + \tilde{\varepsilon}_{s_0}(q_x^c)$, where we have used $\frac{1}{N_a T} \int dt \langle \mathcal{H}_a(t) \rangle \simeq \tilde{\varepsilon}_{s_0}(q_x^c)$, with $\tilde{\varepsilon}_{s_0}(q_x^c)$ the Floquet band obtained from the time-independent Hamiltonian $\tilde{\mathcal{H}}_a$. Using the Langevin equation

$$\langle \dot{c} \rangle = -i \langle [c, \mathcal{H}] \rangle - \frac{\gamma}{2} \langle c \rangle = 0, \quad (\text{S16})$$

we obtain $\tilde{\Delta}_c \alpha^* \alpha = \frac{\tilde{\Delta}_c^2 + \gamma^2/4}{4\tilde{\Delta}_c} \phi^2$. Then the energy density can be written as

$$F = \frac{\tilde{\Delta}_c^2 + \gamma^2/4}{4\tilde{\Delta}_c} \phi^2 + \tilde{\varepsilon}_{s_0}(q_x^c). \quad (\text{S17})$$

Solving the self-consistent equation is equivalent to finding the extremum of the free energy because

$$\begin{aligned} \frac{\partial F}{\partial \phi} &= \frac{\tilde{\Delta}_c^2 + \gamma^2/4}{2\tilde{\Delta}_c} \phi + \frac{\partial \tilde{\varepsilon}_{s_0}(q_x^c)}{\partial \phi} \\ &= \frac{\tilde{\Delta}_c^2 + \gamma^2/4}{2\tilde{\Delta}_c} \phi - \eta_0 \Theta_0. \end{aligned} \quad (\text{S18})$$

Here we have used the Hellmann-Feynman theorem with $\frac{\partial \tilde{\varepsilon}_{s_0}(q_x^c)}{\partial \phi} = \frac{-\eta_0}{N_a T} \int dt dx \langle \Psi^\dagger \Psi \rangle [\cos(k_0 x) + 4\eta_t \sin(k_0 x) \cos(\omega t)] = -\eta_0 \Theta_0$. As a result, $\frac{\partial F}{\partial \phi} = 0$ leads to

$$\phi = \frac{2\tilde{\Delta}_c}{\tilde{\Delta}_c^2 + \gamma^2/4} \eta_0 \Theta_0, \quad (\text{S19})$$

which is nothing but the self-consistent condition in Eq. (4) in the main text.

Stability of the steady states

The stability of the steady state solution can be determined from the dynamical equation of the cavity field Eq. (3) in the main text. Assuming a small fluctuation $\delta\phi = \delta\alpha + \delta\alpha^*$ in the cavity field $\phi = \phi_s + \delta\phi$. Consequently, the atomic density order obtains a fluctuation $\delta\Theta_0 = \frac{\partial \Theta_0}{\partial \phi} \delta\phi$, yielding [6–8]

$$\dot{\delta\alpha} = \left(-i\tilde{\Delta}_c - \frac{\gamma}{2} \right) \delta\alpha + i\eta_0 \frac{\partial \Theta_0}{\partial \phi} (\delta\alpha + \delta\alpha^*). \quad (\text{S20})$$

Eq. (S20) has two solutions taking the form $\delta\alpha = ae^{\epsilon_\pm t} + be^{\epsilon_\pm^* t}$, which are stable (unstable) for $\Re(\epsilon_\pm) < 0$ [$\Re(\epsilon_+) > 0$ or $\Re(\epsilon_-) > 0$]. The system would seek for the steady states that are stable with exponentially decaying fluctuations $\Re(\epsilon_\pm) < 0$, corresponding to the energy minima (maxima) for $\eta_t \ll 1$ and $\Delta_c > 0$ ($\eta_t \gg 1$ and $\Delta_c < 0$), as shown in Figs. S2(c) (d). At the boundary of superradiant phase transition (or the boundary of the hysteresis loop), one of the decay coefficients tends to zero as expected. The transition from zero to finite condensate momentum is characterized by the order parameter q_x^c , thus the decay coefficients of $\delta\phi$ near this transition need not tend to zero.

Experimental consideration

Piezoelectric transducers scheme.—The shaking cavity mode can be realized by mounting two piezoelectric transducers (PZTs) on the two mirrors of the cavity (one on each), and synchronously driving the piezoelectric transducers (PZTs). Alternatively, one can externally drive one PZT and lock the cavity using the other PZT. In this case, the cavity locking and shaking are achieved simultaneously. The servo bandwidth of PZTs are typically of the order of 10kHz, which can be improved significantly using specially designed mounting. For instance, PZTs with servo bandwidth of 200kHz and 500kHz have been demonstrated in experiments [9, 10]. As a result, a shaking frequency up to several hundred kHz can be realized using such PZTs. We can use ^7Li atoms and a high-finesse cavity with a loss rate $\gamma \lesssim 100\text{kHz}$ which can be realized using high reflection mirrors [11].

Electro-optic optical modulator scheme.—The shaking cavity mode can also be realized by inserting two EOMs into the cavity which modify the optical phase delay through tuning the applied voltage. We have considered a high-finesse cavity with a loss rate $\gamma \lesssim 100\text{kHz}$ (correspond to a finesse of 10^4 for a cavity with free spectral range $\sim 1\text{GHz}$). While cavities without EOMs inside can reach a finesse of 10^5 (with round trip loss $< 0.005\%$) in experiments [11]. It has been demonstrated that a highly transmissive intra-cavity element (realized by anti-reflection coating or Brewster's angle incidence) can hardly reduce the finesse of the cavity [12, 13]. As a result, to maintain the high finesse of a cavity with EOMs inside, the EOMs should have extremely low losses (high transmission and low absorption). Using high-efficiency anti-reflection (AR) coating, the reflectivity at target wavelength can be smaller than 0.01% [14], leading to a round-trip loss about $\sim 0.04\%$. Such low reflectivity can also be realized by Brewster's angle incidence [12] (the Brewster's angle would hardly be affected by the applied voltage on the EOM since the change of refractive index is less than 10^{-4}). The absorption of the EOM can be suppressed by using low-absorption electro-optic materials (e.g., gray-track resistance potassium titanyl phosphate crystal or magnesium-doped lithium niobate crystal with an absorption coefficient $\sim 10^{-4}\text{cm}^{-1}$ [15–18]). We also notice that ϕ_0 can be viewed as the phase delay without applying voltage on the EOM, which is used to tune the relative position between the cavity field and the external lattice potential and can also be achieved by shifting the external lattice. Therefore the amplitude of the EOM phase modulation is f which is small $f \sim 0.1\pi$ (enough for our purpose), and the length of the EOM can be reduced to $< 1\text{cm}$ using typical voltage driving (with an amplitude of a few hundred Volts) [18]. The absorption loss per round trip is also of the order of 10^{-4} , which can be improved further by using higher voltage driving since the modulation frequency is only of several hundred kHz). As a result, the total round-trip loss of the cavity can be as low as $\sim 0.05\%$, corresponding to a finesse about 12000. Moreover, to reduce requirement for the finesse, it is also possible to use a longer cavity with smaller free spectral range (FSR), for example, a cavity with a FSR of 0.5GHz only needs a finesse of 5000 to achieve the required loss rate 100kHz .

Gradient driving force scheme.—Finally, we notice that by combining a shaking external lattice $V_{\text{ext}} = v_e \cos^2[k_0 x - f \cos(\omega_0 t)]$ and a periodic driving force from a periodically modulated magnetic field gradient $B = B' x \cos(\omega_0 t)$ [19], it is possible to realize the same Hamiltonian as we proposed. In the co-moving frame of the shaking external lattice, the cavity lattice (static in the laboratory frame) is effectively shaking. Due to the equivalence between acceleration and force [20], the periodic force is canceled out if

$$\frac{f}{k_0} m \omega_0^2 = m_F g_F \mu_B B', \quad (\text{S21})$$

where m is atom mass, m_F is the angular momentum quantum number along the quantized axis, g_F is Lande g-factor and μ_B the Bohr magneton. With these parameters, the amplitude magnetic field gradient should be of the order of 10^6Gauss/m . Currently, periodically driving magnetic field gradient with amplitude 10^4Gauss/m and a frequency of several kHz has been realized [21]. Though in principle this could be improved using better designed (anti-)Helmholtz coils (with more winding turns) and driving current sources (with larger amplitude and frequency), a 10^6Gauss/m gradient with modulation frequency at several ten kHz might be still challenging.

Summary.—The EOM and PZT-driving mirror implementations discussed above are feasible with current technique, while the PZT driving mirror requires a slightly simpler experimental setup than the EOM one. The combination of a shaking external lattice and a periodic driving force would require a more complex setup than the other two and might be still challenging to realize.

* Electronic address: chuanwei.zhang@utdallas.edu

- [1] J. Klinder, H. Keßler, M. Reza Bakhtiari, M. Thorwart, and A. Hemmerich, Observation of a superradiant mott insulator in the dicke-hubbard model, *Phys. Rev. Lett.* **115**, 230403 (2015).
- [2] R. Landig, L. Hruby, N. Dogra, M. Landini, R. Mottl, T. Donner, and T. Esslinger, Quantum phases from competing short-and long-range interactions in an optical lattice, *Nature* **532**, 476–479 (2016).
- [3] J.-S. Pan, X.-J. Liu, W. Zhang, W. Yi, and G.-C. Guo, Topological superradiant states in a degenerate fermi gas, *Phys. Rev. Lett.* **115**, 045303 (2015).
- [4] R. Gehr, J. Volz, G. Dubois, T. Steinmetz, Y. Colombe, B. L. Lev, R. Long, J. Esteve, and J. Reichel, Cavity-based single atom preparation and high-fidelity hyperfine state readout, *Phys. Rev. Lett.* **104**, 203602 (2010).
- [5] A. Yariv and P. Yeh, *Photonics: Optical Electronics in Modern Communications* (Oxford University Press, New York, NY, 2007).
- [6] X.-W. Luo, Y.-N. Zhang, X. Zhou, G.-C. Guo, and Z.-W. Zhou, Dynamic phase transitions of a driven ising chain in a dissipative cavity, *Phys. Rev. A* **94**, 053809 (2016).

- [7] M. J. Bhaseen, J. Mayoh, B. D. Simons, and J. Keeling, Dynamics of nonequilibrium dicke models, [Phys. Rev. A **85**, 013817 \(2012\)](#).
 - [8] D. Nagy, G. Szirmai, and P. Domokos, Critical exponent of a quantum-noise-driven phase transition: The open-system dicke model, [Phys. Rev. A **84**, 043637 \(2011\)](#).
 - [9] D. Goldovsky, V. Jouravsky, and A. Peer, Simple and robust phase-locking of optical cavities with > 200 KHz servo-bandwidth using a piezo-actuated mirror mounted in soft materials, [Opt. Exp. **24**, 28239 \(2016\)](#).
 - [10] T. Nakamura, S. Tani, I. Ito, and Y. Kobayashi, Beyond 500-kHz Bandwidth Piezo-Electric Transducers For GHz-Comb Applications, 2017 European Quantum Electronics Conference, ED-P.4 (2017).
 - [11] B. Nagorny, Th. Elsässer, and A. Hemmerich, Collective atomic motion in an optical lattice formed inside a high finesse cavity, [Phys. Rev. Lett. **91**, 153003 \(2003\)](#).
 - [12] R. J. Jones, K. D. Moll, M. J. Thorpe, and J. Ye, Phase-Coherent Frequency Combs in the Vacuum Ultraviolet via High-Harmonic Generation inside a Femtosecond Enhancement Cavity, [Phys. Rev. Lett. **94**, 193201 \(2005\)](#).
 - [13] A. M. Warrier, J. Lin, H. M. Pask, R. P. Mildren, D. W. Coutts, and D. J. Spence, Highly efficient picosecond diamond Raman laser at 1240 and 1485 nm, [Opt. Exp. **22**, 3325 \(2014\)](#).
 - [14] H. K. Raut, V. A. Ganesh, A. S. Nair, and S. Ramakrishna, Anti-reflective coatings: A critical, in-depth review, [Energy Environ. Sci. **4**, 3779–3804 \(2011\)](#).
 - [15] M. Roth, N. Angert, M. Tseitlin, and A. Alexandrovski, On the optical quality of KTP crystals for nonlinear optical and electro-optic applications, [Opt. Mater. **16**, 131 \(2001\)](#).
 - [16] M. Leidinger, K. Buse, and I. Breunig, Highly sensitive absorption measurements in lithium niobate using whispering gallery resonators, [Proc. SPIE **9347**, 93471D \(2015\)](#).
 - [17] N. Waasem, S. Fieberg, J. Hauser, G. Gomes, D. Haertle, F. Kühnemann, and K. Buse, Photoacoustic absorption spectrometer for highly transparent dielectrics with parts-per-million sensitivity, [Rev. Sci. Instrum. **84**, 023109 \(2013\)](#).
 - [18] A. Yariv and P. Yeh, *Optical Waves in Crystals, Propagation and Control of Laser Radiation* (John Wiley and Sons, New York, 1984).
 - [19] E. Haller, R. Hart, M. J. Mark, J. G. Danzl, L. Reichsöllner, and H.-C. Nägerl, Inducing Transport in a Dissipation-Free Lattice with Super Bloch Oscillations, [Phys. Rev. Lett. **104**, 200403 \(2010\)](#).
 - [20] J. Struck, C. Ölschläger, M. Weinberg, P. Hauke, J. Simonet, A. Eckardt, M. Lewenstein, K. Sengstock, and P. Windpassinger, Tunable gauge potential for neutral and spinless particles in driven optical lattices, [Phys. Rev. Lett. **108**, 225304 \(2012\)](#).
 - [21] X. Luo, L. Wu, J. Chen, Q. Guan, K. Gao, Z.-F. Xu, L. You, and R. Wang, Tunable atomic spin-orbit coupling synthesized with a modulating gradient magnetic field, [Sci. Rep. **6**, 18983, \(2016\)](#).
-